NUMERICAL EVALUATION OF THIN-SHELLED STRUCTURAL PANELS

by

Matthew John Yagodich

Bachelor of Science, University of Pittsburgh at Johnstown, 1994

Submitted to the Graduate Faculty of

the School of Engineering in partial fulfillment

of the requirements for the degree of

Master of Science in Mechanical Engineering

University of Pittsburgh

2003

UNIVERSITY OF PITTSBURGH

SCHOOL OF ENGINEERING

This thesis was presented

by

Matthew John Yagodich

It was defended on

April 8, 2003

and approved by

Dr. Roy D. Marangoni, Associate Professor, Department of Mechanical Engineering

Dr. Dipo Onipede, Jr., Assistant Professor, Department of Mechanical Engineering

Dr. Michael R. Lovell, Associate Professor, Department of Mechanical Engineering

ABSTRACT

NUMERICAL EVALUATION OF THIN-SHELLED STRUCTURAL PANELS

Matthew John Yagodich, M.S.M.E.

University of Pittsburgh, 2003

This paper will provide a basis for the behavior of thin shell corrugated steel structures. Up to this point, the majority of the papers concerning this subject, have been concerned with the analysis of simple arch type buildings. In addition, the panels were treated as flat, curved surfaces. Any corrugation in the panel was either neglected, or was mentioned but not handled in the analysis. Test trials were conducted to evaluate the performance of multi radius panels. A numerical analysis was then conducted to simulate the laboratory tests. The simulation is useful when evaluating larger structures of the same type of panel. The ultimate conclusions that this paper arrives to, is that a linear elastic solution cannot be used to solve problems involving thin shell arch panels. Rather, a non-linear solution is the most precise method for obtaining accurate solutions to the panel in question.

TABLE OF CONTENTS

LIST OF TABLES

Page

LIST OF FIGURES

Page

1.0 INTRODUCTION

1.1 Problem Description

This paper will provide a basis for the behavior of thin shell corrugated steel structures. Up to this point, the majority of the papers concerning this subject, have been concerned with the analysis of simple arch type buildings. In addition, the panels were treated as flat, curved surfaces. Any corrugation, otherwise known as crimp, in the panel was either neglected, or was mentioned but not handled in the analysis.

The cross section for the panel studied for this paper is shown in Figure 1. This style panel, as it currently is shown in Figure 1, can support a building, depending on the location and the configuration of the building, up to 100 feet wide. One of the goals for this project is to optimize the current panel to carry double the current capacity. By evaluating optimum cross sections, a new panel can be designed to achieve this goal. In addition, the role that corrugations play in the panel will also be evaluated.

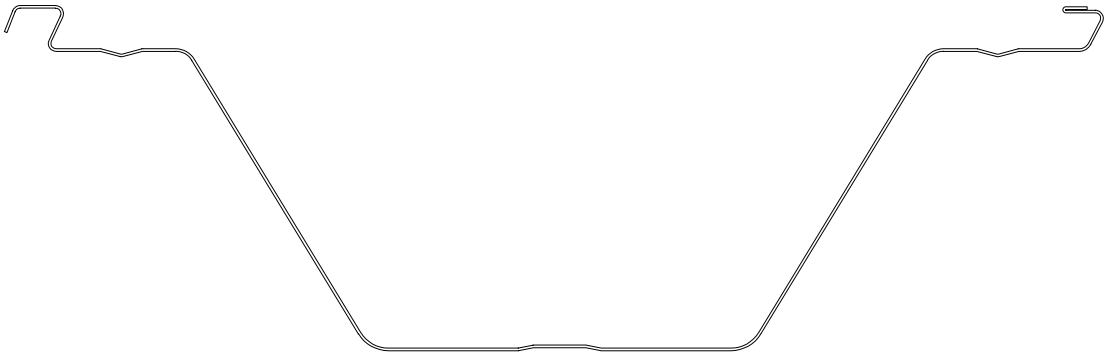

Figure 1 Steel Structural Panel

The corrugations are required in order to facilitate the bending process, however, they are running in the wrong direction for strength. Referencing Figure 1, if one imagines an axis protruding into the paper, which we will call the z-axis, then the corrugations in the panel to facilitate bending are running in a direction perpendicular to this z-axis. This creates crimp that acts as an accordion in the z-axis, or longitudinal plane of the panel. The sides of the panel are also corrugated. The influence that the corrugations have on the structural integrity of the panel needs to be examined in order to make a determination for the overall structures strength. Highly non-linear localized buckling is a concern during the loading of the panels. This paper will attempt to numerically predict the buckling response of this style panel during loading. Once a buckling response is predicted and verified, a new style panel will then be modeled to determine the optimum cross section of the panel, the end result being a significant increase in capacity over the current panel. Figure 2 depicts a detailed view of a typical corrugated panel.

Figure 2 Detail View of Structural Panel with Corrugations

1.2 Literature Review

The literature review contained herein will provide a summary of numerous articles reviewed for content, and more importantly, how the articles in question, provide contributions to this thesis. An attempt will be made, to establish a direct correlation between the attempts to be made in the thesis, and the articles.

The articles chosen for review are based on general shell theory, and how shells react under various loading conditions. There are several articles which have examined the types of buildings constructed from the panels, and how the buildings overall structure is influenced. The main objective for this paper is to establish a correlation between various sizes and shapes of panels. An attempt is to be made to also introduce the effects of the corrugation into the analysis. Although loadings such as snow and wind influence the performance of a building structure, these parameters will not be considered in this paper, nor will they be covered in this literature review.

A paper presented in the Journal of Structural Engineering by Abdel-Sayed, Monasa, and Siddall [1] examined the structural characteristics of cold-formed farm structures, otherwise known as barrel-shells. The structures examined in the paper were of the type known as continuous curvature, meaning the structure possessed a continuous, non-varying radius. Other papers that were reviewed examined similar structures. The analysis process in this paper consisted of classical orthotropic cylindrical shell theory that was backed up by physical tests. It should be noted that the structure tested was of the bolt-together type. The structures involved in this thesis are seamed panels containing no bolts or fasteners of any kind. A detail of the shell

analysis will not be discussed here. Rather, a summary of the calculations in the paper will be discussed. A closed form solution describing the variance of the crimp along the panels' length at various radii was established. This leads into formulae that describe the panels' axial rigidity. The author suggests that the cross-corrugations on the panel have significant effect on the performance and rigidity of the panel. They improve its local buckling characteristics and reduce its bending and axial rigidity in the curved direction. Because the panel being investigated in the thesis can have varying curvature throughout the length of the panel, the solution for rigidity of the panel will play an important role in the analysis. The article goes on to further suggest that the panels were shown to fail by buckling of the "web" portions. The physical panel tests showed that the panel yielded well before the ultimate load of the panel was reached. The author makes an assumption by stating that panel failure occurs when the compressive yield is reached in the zone of shallow corrugations, or when the expected limit of plastic deformation occurs in the deepest corrugations. A mention of residual stresses is also brought up as a possible key player in the failure of the panels. Numerous equations are derived for non-linear buckling load determinations, which could be used as a comparison tool during the analysis runs conducted later in the thesis. The last noteworthy comment to make is that the author mentions that due to the panels being bolted together, and end walls being used at the ends of the building, a single panel can be analyzed as a thin shell supported an all four edges. This is a very important observation to make due to the desire to drive the efficiency of the finite element model to a higher point, which includes, properly applying accurate boundary conditions. Twenty-six references were cited in this paper.

As a compliment to the above reviewed paper, an article published in the Journal of the Structural Division by El-Atrouzy and Abdel-Sayed [2] describes the prebuckling analysis of orthotropic barrel-shells. The paper details how to calculate the rigidities of the panel. The two areas that control and influence the rigidities of a panel are the material and geometric parameters of the sheets. The paper also details the particular and homogeneous solutions to the governing differential equations describing orthotropic shell theory. The homogeneous solutions to the equations were obtained from tests taken on actual test buildings. The only type of building tested was of the continuous curvature type. The buildings that will be evaluated in this thesis can contain non-continuous curvature buildings. Therefore, the homogenous portion of the solution found in this paper cannot be used as a tool for non-continuous buildings. An interesting hypothesis to pose however, is whether or not superposition can be used to evaluate a non-varying continuous building by adding up the components of the building in question. In all, the following conclusions have been drawn in this paper. The linear solution will always predict a higher value than the non-linear solution. The prebuckling method produced the most agreeable solution between the experimental results, and the analytical solution. Eight references were cited.

A third paper published in the Journal of Engineering Mechanics by Bagchi and Paramasivam [3] is noteworthy from the standpoint that the paper discusses the possibility of using a linear eigenvalue solution to predict the nonlinear buckling response of the panel. The idea is to properly combine the linear buckling analysis and geometrically nonlinear prebuckling analysis with the minimum number of load steps. The general idea could possibly be used in this paper from the standpoint that the timesavings in the FEM model would be reduced by utilizing

the methods presented in this journal article. Since non-linear solutions are traditionally very expensive numerically, a linear eigenvalue solution may be a viable option when conducting optimization studies. Eleven references were cited.

A fourth paper published by the Journal of Structural Engineering by Pi and Trahair [4], discusses the effects of In-Plane buckling on a thin-shelled panel. The paper also mentions the effects of residual stresses, and how these stresses might affect the performance of the panels. The entire article discusses the results of numerically derived pin ended arches, both shallow and high arches. Classical elastic buckling theory was used in comparison to non-linear inelastic models. In all cases, the classical buckling theory was shown to overestimate both the bifurcation and the snap-thru buckling loads for shallow pin-ended arches. The non-linear numerical solution was shown to provide a more accurate solution to the buckling problem of the arches buckling in plane. This finding collaborates the research performed by El-Atrouzy and Abdel-Sayed [2]. In addition, the article discusses that standard code practices for evaluating steel beam-columns cannot be used for evaluation of arches. Again, a non-linear numerical solution is the suggested method for an accurate solution. The paper concludes with equations being offered to solve arch structures, while taking into account the non-linear affects inherent in the structure. Thirty-two references were cited.

A paper published by the Journal of Engineering Mechanics by Bradford, Uy, and Pi [5] discusses the In-Plane stability of arches under a concentrated load. This article is important from the standpoint that a wealth of detailed derivations for closed form solutions of non-linear equilibrium differential equations are presented and discussed. In addition, a rigorous

mathematical derivation is presented detailing the buckling characteristics of numerous types of arches. Unlike the Pi and Trahair [4] paper, Bradford, Uy, and Pi evaluate both pin ended and fixed ended arch structures. The author states that the comparisons between finite element models and the closed form solutions presented are reasonably accurate. Lastly, a criterion for using the closed form solutions for the study of full arches with concentrated loads is presented. This paper contains over twenty references.

A report published by the US Army Corps of Engineers by Sweeney, Briassoulis, and Kao [6], discusses the results of several full-scale tests performed on a thin shell arch building. The method of test was discussed in detail. One overwhelming conclusion the authors present, is that the arches in all cases were shown to fail through the formation of collapse mechanisms, or hinges. At the onset of a hinge, the structure was shown through moment redistribution to establish additional hinges until overall failure of the structure occurred. The paper is worth noting here in that, if further work is to be conducted on full arch structures, the overall in-plane buckling mode of failure should not be ignored. Over ten references are cited.

In addition to the reviews and papers listed here, the bibliography section of this paper features numerous other papers and references containing valuable information on thin-shelled buckling analysis that the reader may find of interest. The papers include discussions concerning analytical and numerical procedures, physical testing, and recommendations for future analysis and verification.

1.3 Outline of Work

I. Experimental

- A. Test Rig Setup
- B. Test Methods
- C. Data Collection
- D. Experimental Results

II. Finite Element Model

- A. Geometry
- B. Material Properties
    1. Material Property Modification
- C. Boundary Conditions
- D. Loading
- E. Results Verification

III. Optimization

- A. Other Geometries
- B. Discussion

IV. Conclusions

- A. Recommendations

2.0 EXPERIMENTAL

2.1 Description of Apparatus

In order to test the current panel configuration to determine the strength, a testing station was established. The station was designed to accept a panel in a 4-point bend test configuration. A general overview of the testing stand is shown in Figure 3.

Figure 3 Testing Stand Setup

As shown in Figure 3, the stand was constructed from structural steel. Two main uprights containing a V shaped notch at each end with a roll bar spanning between them was used to support the two ends of the panel. The roll bar was used to provide support in the vertical direction, and yet allow the panel the ability to rotate about the axis of the roll bar. This condition allowed the panel to be completely free of any moments at the ends. Figure 4, depicts the test piece with all the accessories for performing the test attached.

Figure 4 Test Setup Shown With Loading Cage and Connecting Arms

Figure 5 Loading Rig With Load Cell Attached

The test cage consisted of structural steel with two solid steel rods inserted through holes in the top of each of the four corner uprights. The steel rods were placed above the test panel, and allowed to rest freely on top of the panel. The bottom of the loading cage consisted of four link arms that were connected to the four corner uprights. Two link arms on each side of the loading cage were then connected underneath the cage in the middle. A solid steel piece of round stock was then straddled between the link arm connections. The round stock had an eyelet welded to the middle of the piece. Connecting arms were then attached to the eyelet via a lifting clevis. The other half of the connecting arms were attached to a custom built clevis, which was designed to thread into the opening on a load cell. Figure 5 shows the setup with the load cell attached.

The load cell is connected between two threaded, custom made clevises. The bottom clevis was then attached to a hydraulic cylinder. The load cell was directly connected to a data acquisition system designed to read and record data streaming from the load cell in real time. In addition to reading the load the hydraulic cylinder was placing on the panel test piece, a linear displacement potentiometer was also connected to the panel. Figure 6 shows the custom setup for the displacement transducer.

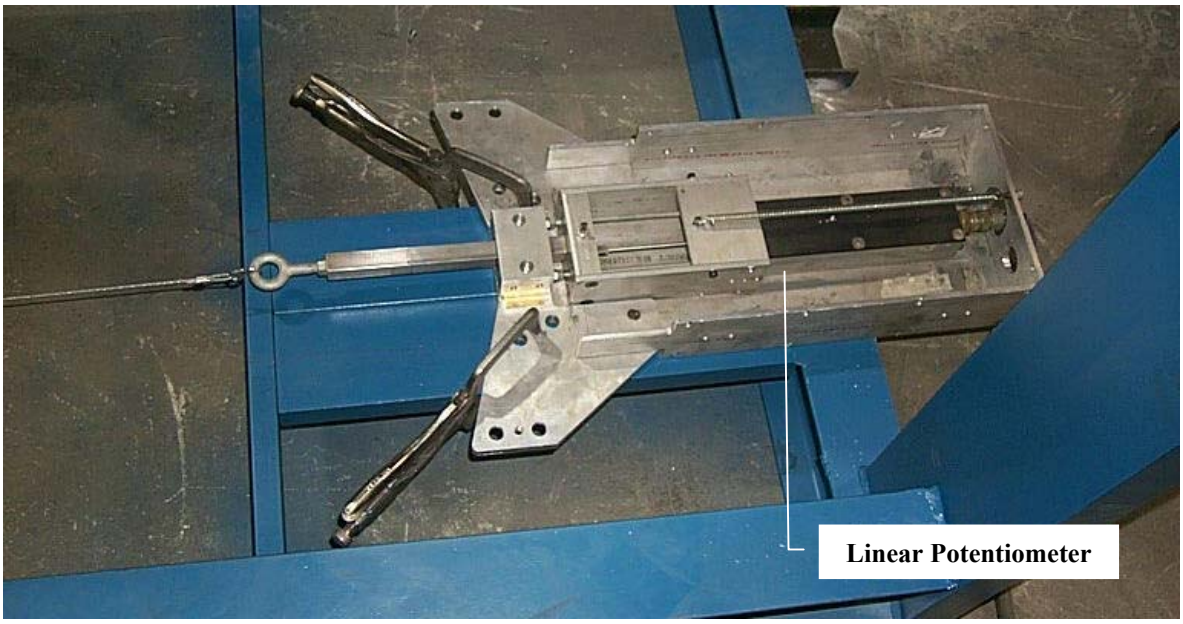

Figure 6 Linear Potentiometer Housing and Associated Cable/Pulley System

Figure 7 Linear Potentiometer Magnet

The potentiometer was placed in a housing so as to better stabilize the unit. A cable was connected to the end of the potentiometer, and ran thru a pulley located directly below the center

portion of the test panel. The cable effectively made a 90° turn and was attached to the test panel thru the use of a magnet, as shown in Figure 7. The potentiometer was connected to the same data acquisition system as that of the load cell. To further stabilize the panels, plates were attached to the panel by using Tek screws and fastening the plates directly to the test panel. The plates were manufactured from the same material as that of the test panel. They were placed in the vicinity of where the main loading rounds came into contact with the panel. Figure 8 depicts a detailed view of the stabilizing plates.

Figure 8 Detail View of Stabilizing Plate

As shown in Figure 8, the stabilizing plates were placed in directly the mid line-loading plane of the loading cage. The plates accurately simulated the panels as they are used in a service condition. The plates were used to stabilize the panel against out-of-plane buckling, which does not occur in a service condition.

2.2 Testing Methods

The test was conducted in a classical four-point bend configuration. The test piece was placed between two support rods, which were designed to allow rotation. All test pieces were loaded in the negative bending configuration. The rotation of the support rods ensured that the test piece had no moment at the supported ends. A loading cage was designed such that the cage could accept the test panel by lifting the cage up and underneath the test panel. The cage was lifted such that the four top corners of the cage were protruding above the test panel in the middle of the test piece. There were four holes, one in each corner leg, whereby two loading rods were inserted through each side of the loading cage. The rods were then allowed to rest on top of the test panel, effectively allowing the test cage to hang underneath the test panel. A modified clevis was attached to a pull lug on the test cage, while the other end of the clevis had an allowance for a load cell to be threaded into it. On the other side of the load cell was another modified clevis, effectively connecting the apparatus to a hydraulic cylinder. The load cell was a tension/compression type load cell. For the testing, the load cell was set up to read only in tension. This was done to increase the resolution of the unit to its maximum range. The hydraulic cylinder was connected to a portable hydraulic unit consisting of a motor, valve bank, pump, and reservoir. This provided the hydraulic power necessary to run the cylinder. An adjustable control valve was coupled to the main hydraulic valve to provide accurate control of the flow of hydraulic fluid to the cylinder. The flow was controlled by allowing the main hydraulic valve to be in the full open position, while having the adjustable valve initially in the full closed position. By slowly opening the adjustable valve, the flow of hydraulic fluid could be accurately applied to the hydraulic cylinder. A laptop computer was used to record the data as the panel was loaded. The load cell provided an output of between 0 and 10 volts, which was conditioned in the data

acquisition system to read as an output of pounds force. The transfer of the force was directly through the load cell and into the clevis pulling on the loading cage attached to the test panel. Caution was used to ensure that a pure tensile pull at the load cell was achieved. In addition, due to the use of the clevises, the load cell was also self-centering, also allowing and ensuring a pure tensile pull at the load cell. As hydraulic pressure was slowly released to the cylinder, the data acquisition system was constantly being monitored for activity. Two separate channels were being monitored simultaneously. One channel was for the output from the load cell, and the other channel was output from the potentiometer. The data was streamed directly to a text file in two separate columns. The panel was loaded until failure occurred, at which point the data stream was halted, and a new panel was loaded into the test fixture. There were a total of 27 tests conducted. The panels can be curved at varying radii. The process is performed by allowing either deep crimp to produce a tight radius, or by allowing loose or virtually no crimp for a straight panel. The effects of the crimp and the radius of the panel are very important in determining the overall width of the structural panel.

Table 1 Summary of Structural Panel Test Configurations

Test Data Summary	
Tested Radius	**Number of Tests**
15 ft.	6
25 ft.	6
50 ft.	6
Curved (Crimp)	6
Straight	3

The configuration was based on a target material thickness of 0.060 inches. The actual material thickness used for the test, as measured by a micrometer, was 0.063 inches. This amount

of data is deemed significant enough for confirmation of the finite element model. Upon verification of the finite element model, an optimization analysis will be conducted to determine the optimum geometry for the panel.

2.3 Experimental Results

The following section details the results of the physical testing. As mentioned earlier, there were a total of 27 tests conducted on 0.060-inch nominal material. All the tests were negative bending tests. Graphs were generated for each set of individual tests and plotted to produce load-deflection plots. The results of the plots are shown below. Due to the material being considered proprietary and classified, the plots shown in this paper are all normalized. As one can clearly see, the relationships are all non-linear in nature. This confirms the several articles reviewed earlier stating that a pure linearized solution cannot be used to solve the problem from a numeric standpoint. Based on this result, it would appear that to perform a numerical analysis for these types of panels, a non-linear analysis must be used to obtain an accurate solution.

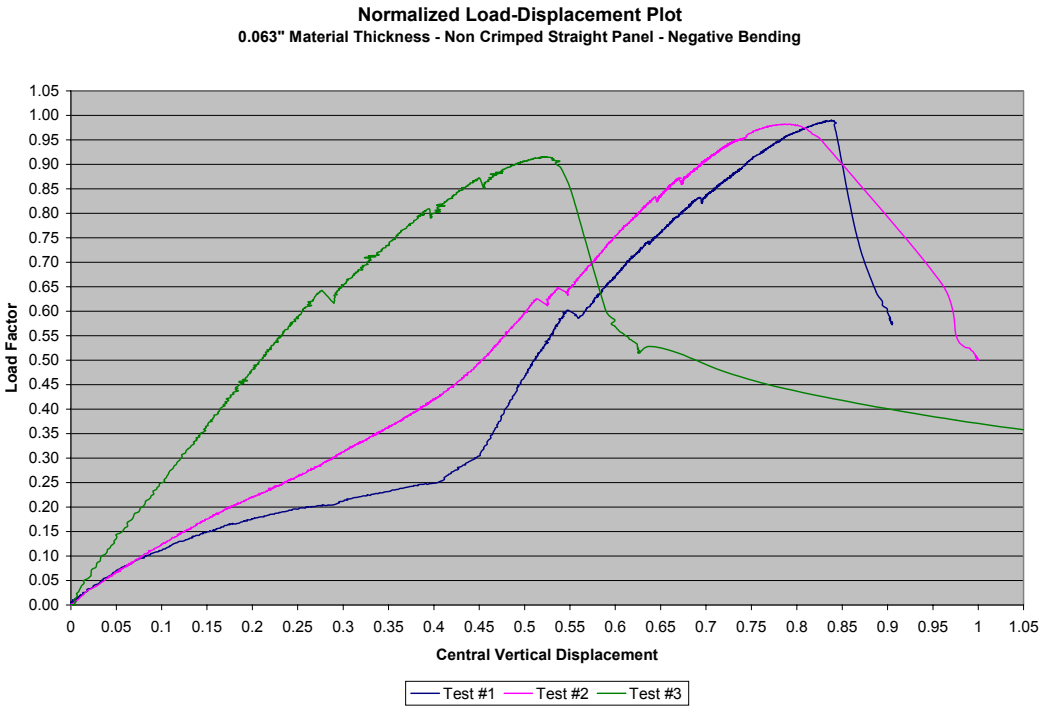

Figure 9 Load-Displacement Plot: Straight Panel with No Crimp

As shown in Figure 9, the test for the straight panel with no crimp (i.e. a panel with no corrugations) shows the behavior of the panels. One will notice a stiffening effect occurring to two of the panels, evidenced by the relatively low slope of Test #1 and Test #2. Test #3 does not appear to exhibit this behavior since the slope upon initial loading increases without losing any stiffness. It shall be shown and discussed in other tests that the phenomenon of stiffening is predominating in how the panels react.

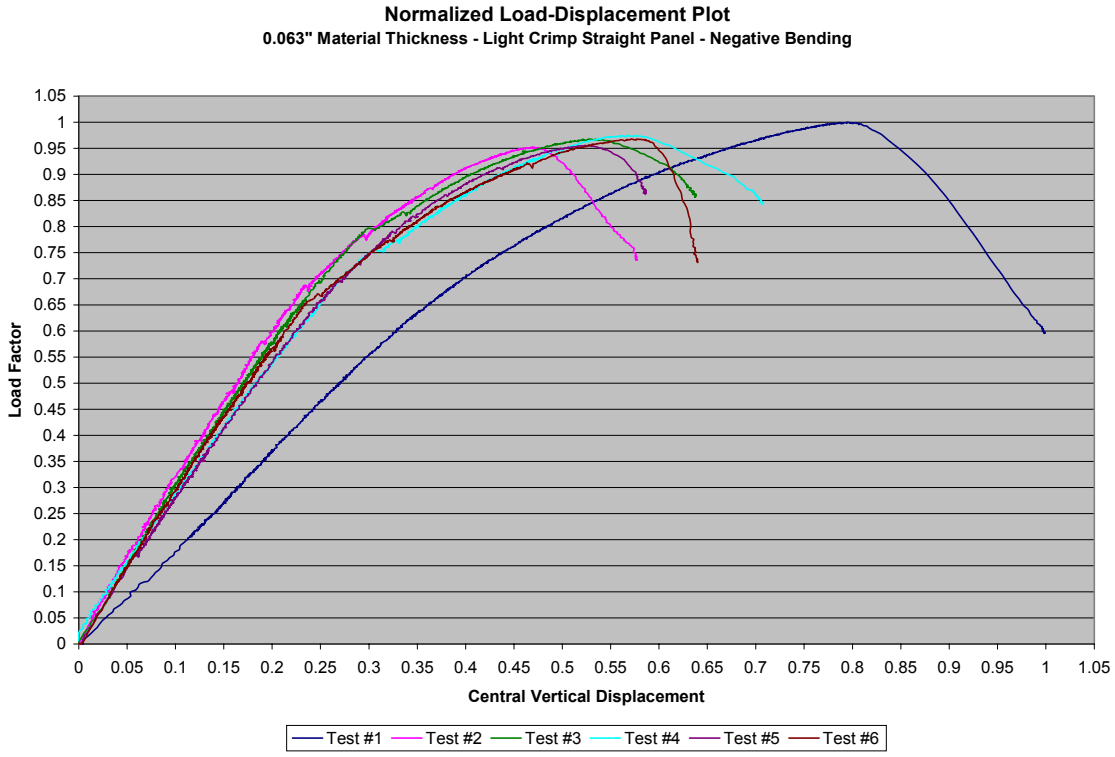

Figure 10 Load-Displacement Plot: Straight Panel with Light Crimp

Figure 10 shows load-deflection curves for a straight panel with very light crimp introduced into the panel. A total of six tests were performed in this series. As shown, five of the six tests follow the same trend. Test #1, shows a deviation from the norm as evidenced by the lower slope. One will also notice that Test #1 gains a slightly higher load than the stiffer panels.

This may be a result of the effects of how the panel relaxes or deflects during the loading procedure. This will be discussed in future loadings.

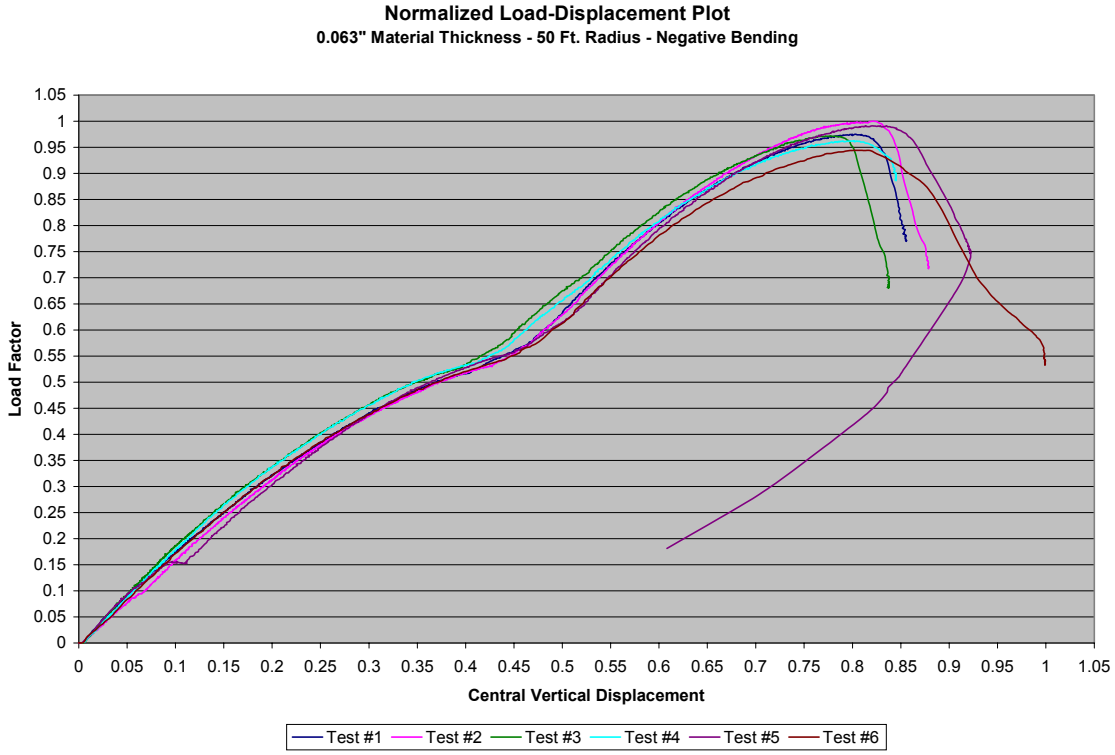

Figure 11 Load-Displacement Plot: 50-Foot Radius Panel

Figure 11 shows a test series consisting of 50-foot radius panels. As was discussed previously, this test series also depicts the stiffening phenomenon during the loading of the panel. In this case, all six test cases show this effect. At approximately one half the maximum load, the curves reverse themselves and actually begin to accept more load by stiffening. As mentioned, the theory behind why this may be occurring concerns the possibility that as the panel accepts load, a small deformation occurs within the panel structure itself. This deformation, in conjunction with the crimp existing in the panel, may provide an answer to explain the stiffening effects seen in the panels during loading. Because the loading conditions were such that the panel was allowed to freely move across the rolls in the testing cage, it is

doubtful that the test setup itself introduced any inherent adverse affects into the panel. As shown in Figure 12, the stiffening can again be shown.

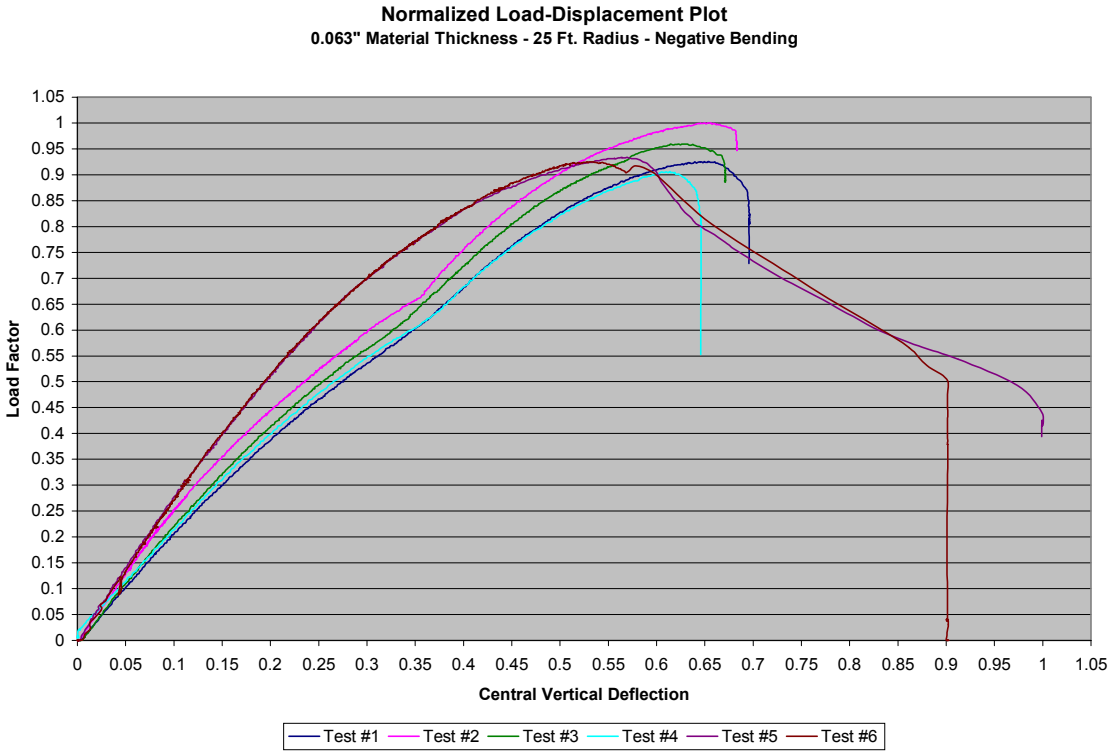

Figure 12 Load-Displacement Plot: 25-Foot Radius Panel

In the case of the twenty-five foot radius test series, four out of the six tests depicts the stiffening effects. The last test series to be conducted, involved fifteen-foot radius panels. The results of this test series are shown in Figure 13. In Figure 13, one can see that the stiffening effects are predominately not shown to appear during the test. Test #2 however, does show an interesting anomaly at nearly one half the maximum applied buckling load. One can notice a sudden and rather large drop off in load, at which time the panel recovers and continues to take on more load. As seen previously in the cases where stiffening was shown to occur, the panel is able to recover and continue to take load to a maximum value at or near the maximum values of the panels that do not exhibit stiffening effects at the middle load of the panel.

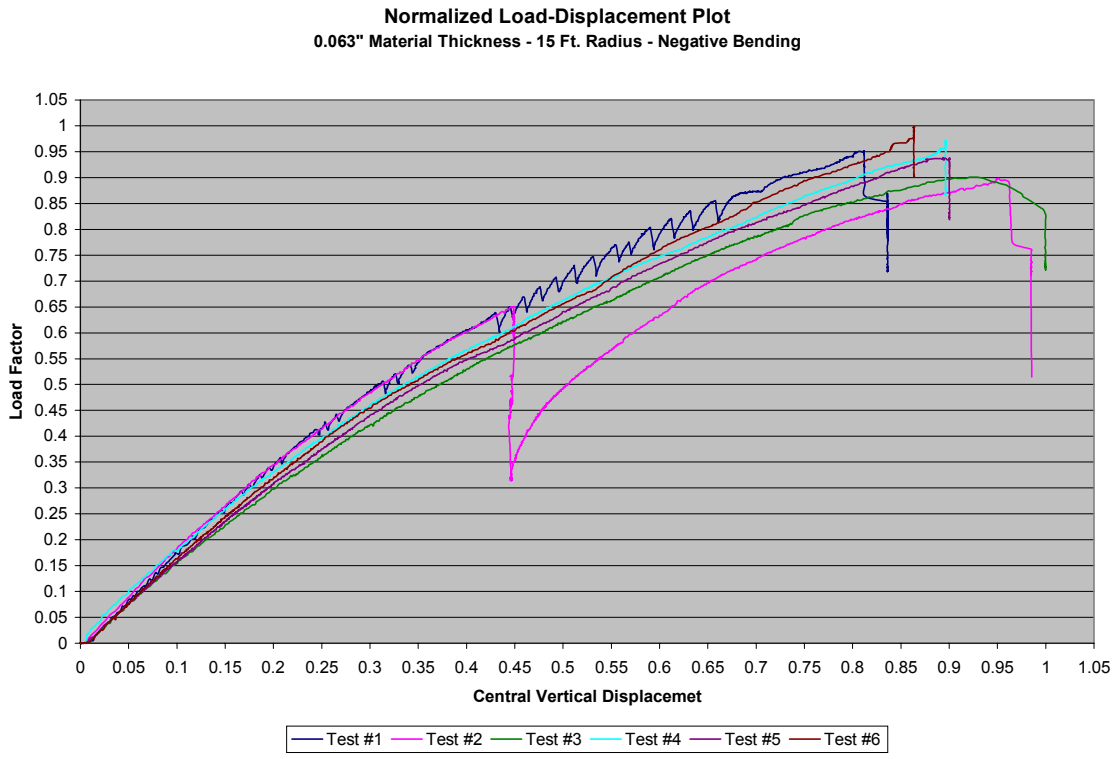

Figure 13 Load-Displacement Plot: 15-Foot Radius Panel

It should also be mentioned, that all the tests failed in the region between the two loading points. This is to be expected for a four point bending test. Localized buckling was the primary mode of failure for the test pieces. Figure 14 depicts a typical failure. As shown, the failure occurs towards the center of the two loading bars as seen on the top, or belly, of the panel. The sides of the panel, as well as the belly itself, show signs of localized buckling. The next section discusses the numerical solution using an eigenvalue solver to predict the localized buckling of the panels. One will notice that the numerical prediction is accurate in terms of the predicted modes of failure. Figure 15, depicts a straight panel failure lying on the ground showing the inside portion of the panel. One can also take note, the detail of the stiffening plates added to the panel at each of the loading points to prevent premature torsional failure.

Figure 14 Detailed View of Localized Buckling Failure

Figure 15 Detailed View of Localized Buckling with Stiffening Plates

3.0 FINITE ELEMENT MODEL

3.1 Geometry

The finite element model geometry was conducted in two phases. One general approach is to use a linearized eigenvalue solution for the problem. Based on analysis conducted for this paper, it can be suggested that if a corrugated panel (any panel for that matter) is modeled explicitly and an eigenvalue solution is extracted from the explicit model, a relatively accurate solution can be obtained. Based on this information, an explicit model was developed which appears to support this theory. Using shell elements, a model of the panel was obtained. The shell elements allowed the panel to be geometrically accurate, with the exception of the corrugation. This solution will be useful when developing a new panel which does not yet possess any test data depicting its' performance. Rather, this method can be used to obtain a "target" load that can then be used to design the actual panel for testing. By evaluating numerous explicit models, a geometry can be chosen which offers the highest predicted buckling load. From these studies, a comparison between different panel styles can be relatively quickly analyzed.

A second model was developed for analyzing the response of the panels during the physical testing phase. 3-D beam elements were utilized to analyze the tested panels. The cross section of the panel was inputted and assigned to the beam element. This method was utilized due to the efficiency of performing the non-linear calculations. An explicit model, as mentioned above, is too large and thus does not lend itself to an efficient non-linear solution. The linearized eigenvalue solution is trim enough to perform the calculations in a relatively short amount of time, and still provide a roughly good estimate of the prebuckling load.

3.2 Material Properties

The material properties used for the explicit finite element solution were what could be considered standard material parameters for mild steel. The modulus of elasticity assigned was $29x10^6$ psi, and Poisson's Ratio was set to 0.3. These material properties were assigned to the shell elements and used for the eigenvalue analysis. The material thickness of the panels were directly assigned to the shell elements upon completion of the meshing process. The assigned material thickness was 0.063 inches, which matched the actual test panels.

The material properties assigned to the non-linear models using 3-D beam elements were a modified stiffness curve. Each panel, depending on its' radius, was assigned a different stiffness curve. This method was necessary due to the crimp of the panel affecting the performance of how the panel actually behaves. The process for programming the curves was established by evaluating the non-linear solution, and superimposing the solution onto the actual test load-deflection plots. The stiffness curve was then adjusted until the non-linear solution matched the test data. This method was performed for each set of different radius panels. By using this method, and assuming one has access to actual test data, a stiffness curve for the panel can be established which describes the performance of the panel, while taking into account the effects of the highly non-linear effects of the crimp in the structural panel. In addition, any possible stiffening effects arising from the loading of the panel can also be captured in the user defined stiffness curve.

3.3 Boundary Conditions and Loading

The boundary conditions for the explicit solution were modeled after the same type of boundary conditions that existed in the actual physical testing. The ends of the panel were constrained to restrict the panel from translating in the vertical downward direction. The loads were applied in the y-axis direction. Both ends of the panel were fixed in the y-direction to prevent the panel from translating in the normal direction during loading. The edges along the top flange of the panel on each end were also fixed to prevent movement in the transverse direction of the panel. This was done to simulate the round rollers supporting the panels' outer flanges during the actual test to prevent premature failure of the upper flange. Nodes restraining the movement in the x-direction were also employed to simulate the stiffening plates used during the actual testing to prevent premature buckling outside the loading zone. This methodology was also used to constrain nodes along the middle portion of the panel where the loading cage channel supports were located. Again, this boundary condition was imposed to simulate the stiffening plates discussed in the testing methods section. The rest of the panel nodes along the two edge flanges were allowed to deflect. The forces were set as a whole to unity and were placed in the same locations with respect to the ends of the panel as they were in the actual test. The total number of nodes to be loaded were summed up, and then divided out by one to achieve a unity loading condition. The loads were in the positive y-direction, and were placed across the belly of the panels. Care was taken not to load any nodes that were in the flange of the panel. The location on the panel model was along the bottom web of the panel, again, as was done in the actual test. To provide a solution, a linearized eigenvalue buckling analysis was utilized. Figure 16 shows the details of the boundary conditions and loading conditions.

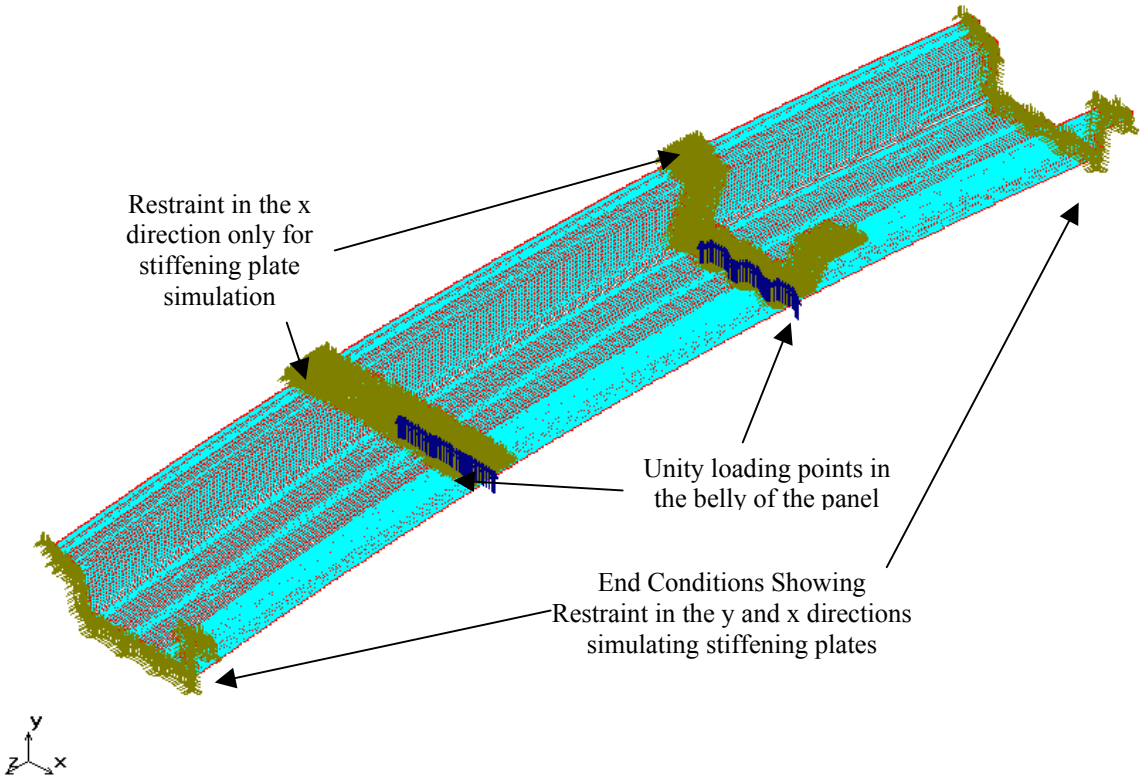

Figure 16 Detailed View of Boundary Conditions for Explicit Model

The 3-D Beam Element model boundary conditions were similar to the explicit model in terms of the ends being constrained in the plane of loading. The far left node was also fixed in the longitudinal direction, while the far right node was allowed to translate in the longitudinal direction. To provide in-plane stability to the model, all nodes in the transverse direction were constrained. This boundary condition ensured that no failure could occur in the out of plane buckling mode. At the proper intervals, two point loads were placed. The loads combined added up to a unity loading condition. To provide a solution, a non-linear scheme was utilized. Unlike the explicit eigenvalue solution, which captures localized buckling of the panel, the 3-D beam element model was based on the assumptions that there is no localized buckling, and the effects of large displacements are present. To capture any discontinuity associated with the effects of strain hardening, or any other phenomenon, a Newton-Raphson procedure in conjunction with an

arc length control method was selected as the method for a solution of the non-linear equations. This method will ramp up the loads starting from unity and automatically adjust the arc length of the solutions' load-displacement curve according to the stability of the panel. The loads are adjusted automatically until equilibrium in the panel is restored for each load step. Figure 17 depicts the boundary and loading conditions.

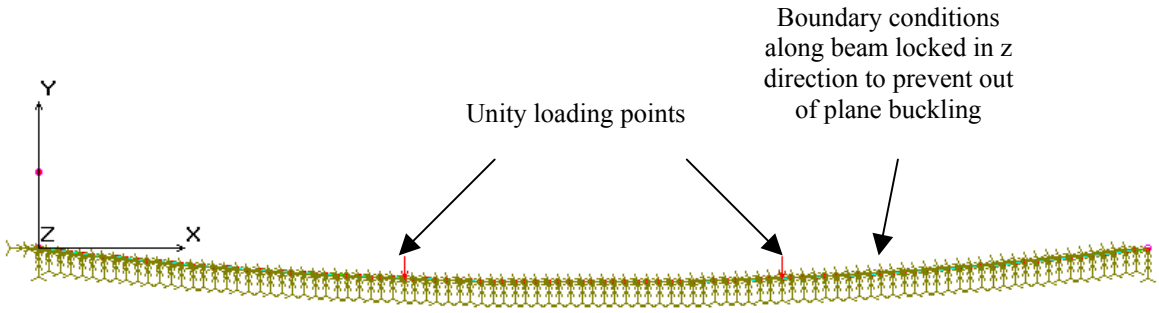

Figure 17 Boundary and Loading Conditions for Beam Element FEM Model

3.4 Results and Verification

The first task attempted was to perform a linearized eigenvalue buckling analysis of a panel having a known loading history, which was obtained through testing. The goal was to validate if an eigenvalue solution would yield a result that would match the test results within reason. The solution for a typical panel is shown below.

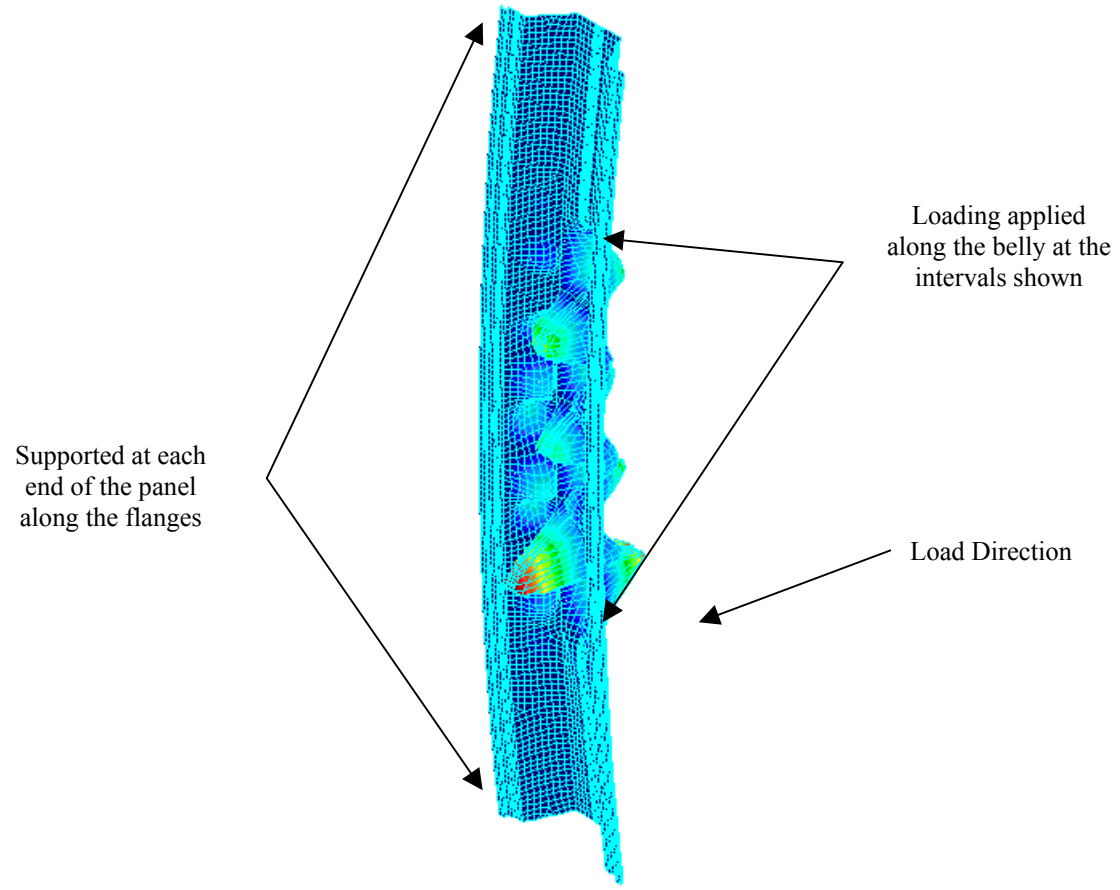

Figure 18 Typical Eigenvalue Solution for 4 Point Bend Test (Negative Bending)

As mentioned earlier in this paper, the actual result is not shown due to the loads being proprietary information, however, Figure 18 depicts the buckling mode that does match the actual buckling mode seen during the testing. The localized buckling is shown to occur between

the two loading points, which in this case, were placed in the middle of the panel. The predicted load did on a consistent basis come to within fifteen percent of the load seen during the testing. This solution was utilized to obtain a buckling load for a straight, fifty-foot radius, and a fifteen-foot radius panel. In all cases, the boundary conditions and methods of loading were consistent. The predicted solution was also confirmed in all cases to be within at least fifteen percent of the actual load.

The results of the non-linear analysis were calibrated to fit the actual test data. The process was performed by programming a modified stiffness curve that produced a load-displacement curve that matched the load-displacement curves from the actual tests. This process was very important since it shows that the tests can be duplicated numerically. Upon duplication of the material properties for a panel possessing a certain radius, it would then be possible to program the modified stiffness curve into a non-linear solver, and predict the response of any size panel. The results for the predicted numerical solution are shown in the plots below.

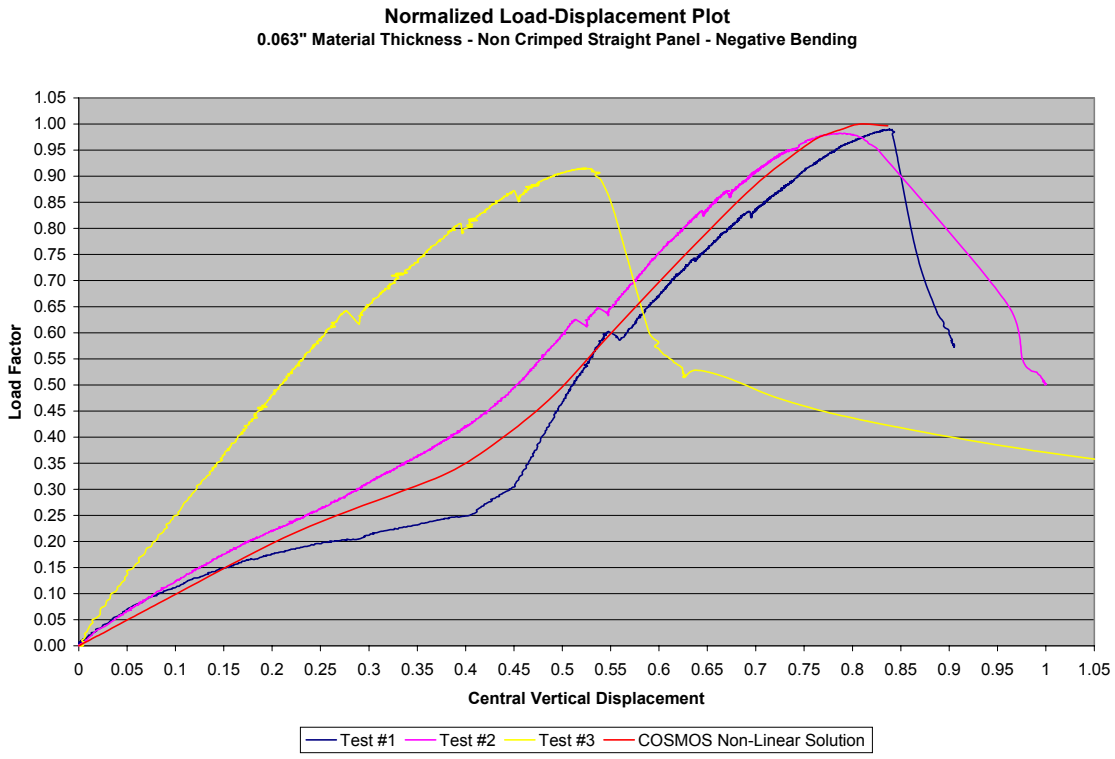

Figure 19 Load-Displacement Plot: Straight Panel with No Crimp w/Numerical Prediction

Figure 19 depicts the original load-deflection curves for a straight panel with no crimp. As mentioned earlier, the numerical solution was obtained by modifying a stiffness curve to match the test data. The modification of the material properties is necessary to account for any material non-linearities occurring in the panel during loading. In Figure 19, the red line designates the numerical solution. Test #3 in this case was essentially not included in the averaging for the solution of the computer model. This test is not considered to be representative of typical panel behavior.

Figure 20 depicts the solution for a straight panel with light crimp. Again, the same procedure was used to extract a non-linear solution to the test data. The majority of the tests all

comply to within expected boundaries for deflection and load, as shown by the tight grouping of the tests.

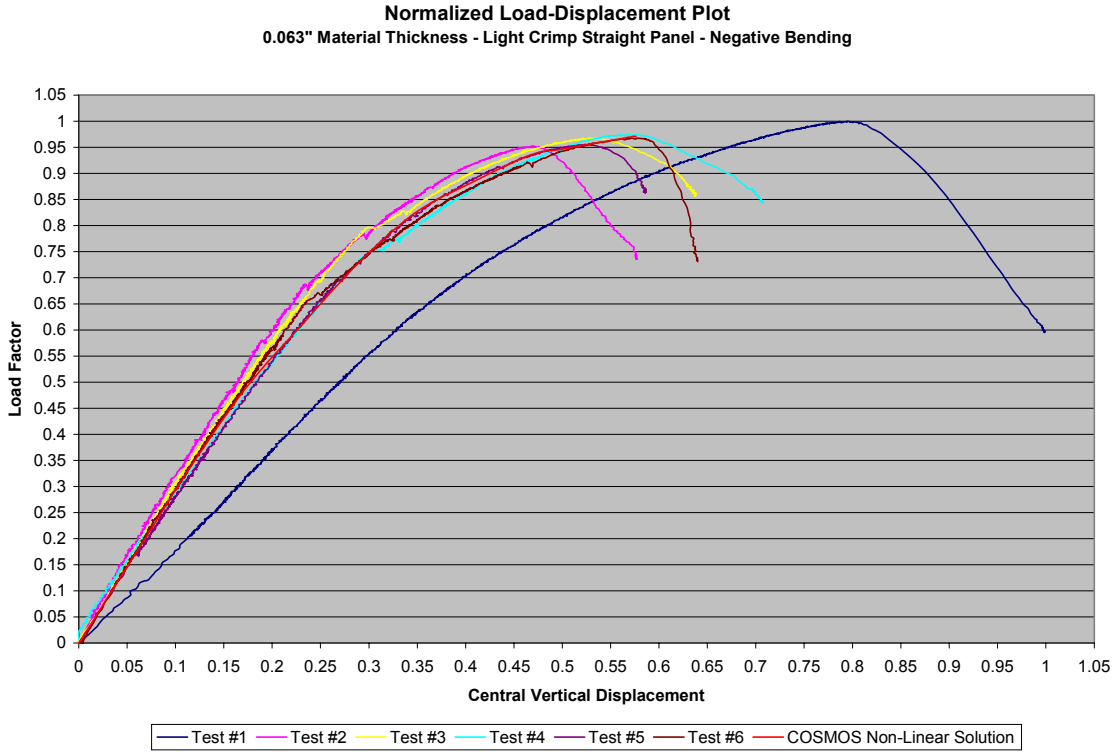

Figure 20 Load-Displacement Plot: Straight Panel with Light Crimp w/Numerical Prediction

As was seen in the straight panel tests with no crimp, there is a case for the light crimp test series whereby one test did not comply with the normal load-displacement relationship. This case was Test #5. As was done in the previous test series, Test #5 was not included in the modification of the stiffness curve for a solution, since this test does not comply with the normal solution mode. The numerical solution extracted from the non-linear analysis is again shown in red.

Figure 21 shows the solution for a fifty-foot radius panel. Very good agreement between the test data and the numerical solution exists for this test series. The stiffening phenomenon that was discussed earlier was also successfully modeled into the numerical solution.

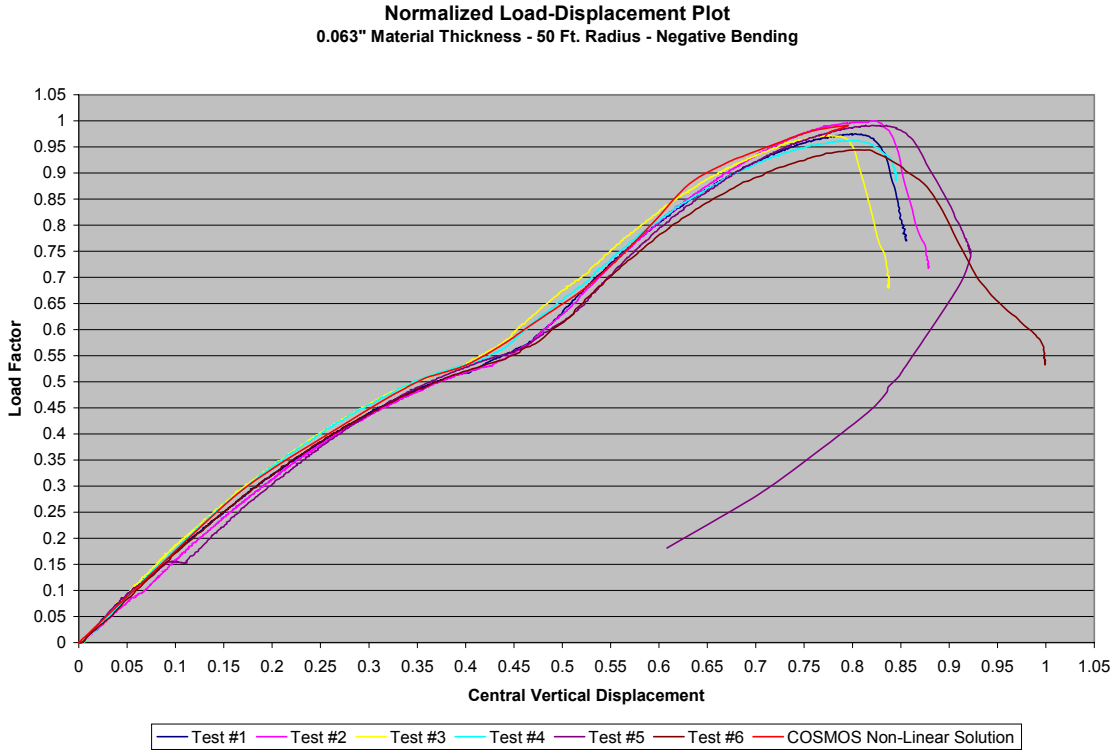

Figure 21 Load-Displacement Plot: 50-Foot Radius Panel with Numerical Prediction

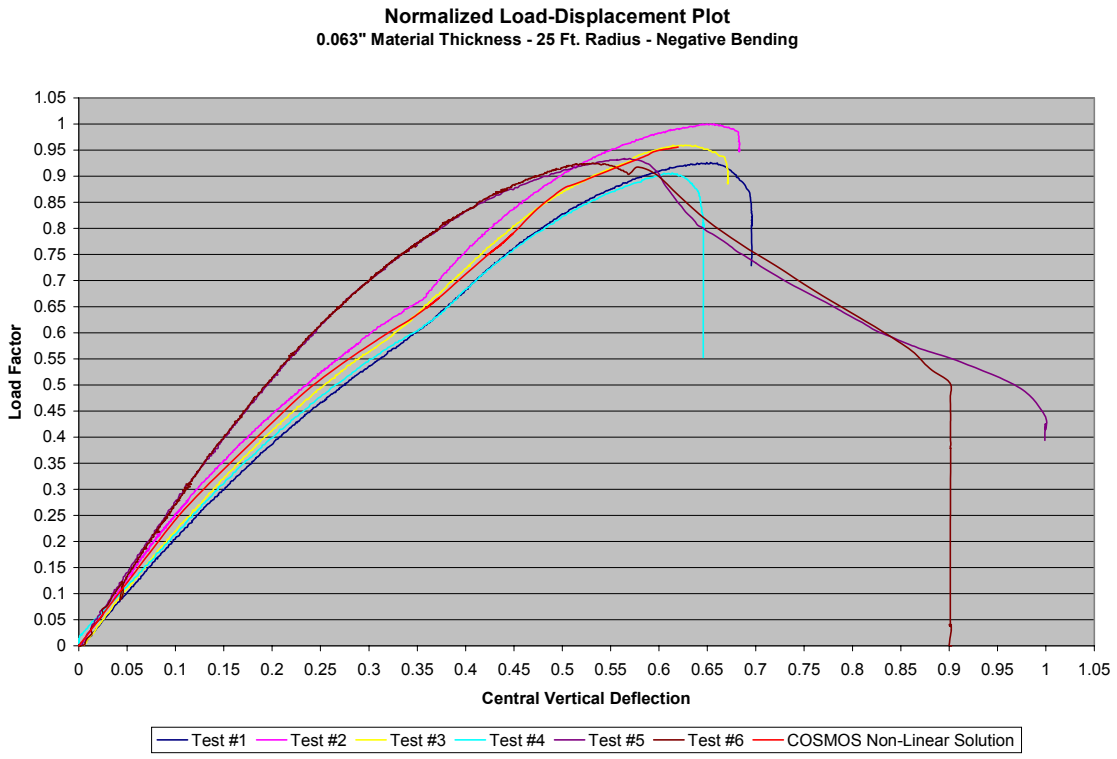

Figure 22 Load-Displacement Plot: 25-Foot Radius Panel with Numerical Prediction

Figure 22 represents the solution for a 25-foot radius panel. In this test series, Test #5 and Test #6 were somewhat stiffer from the other four tests. Again, as was done previously, the numerical solution was modeled to the norm for the panel behavior seen in the actual testing.

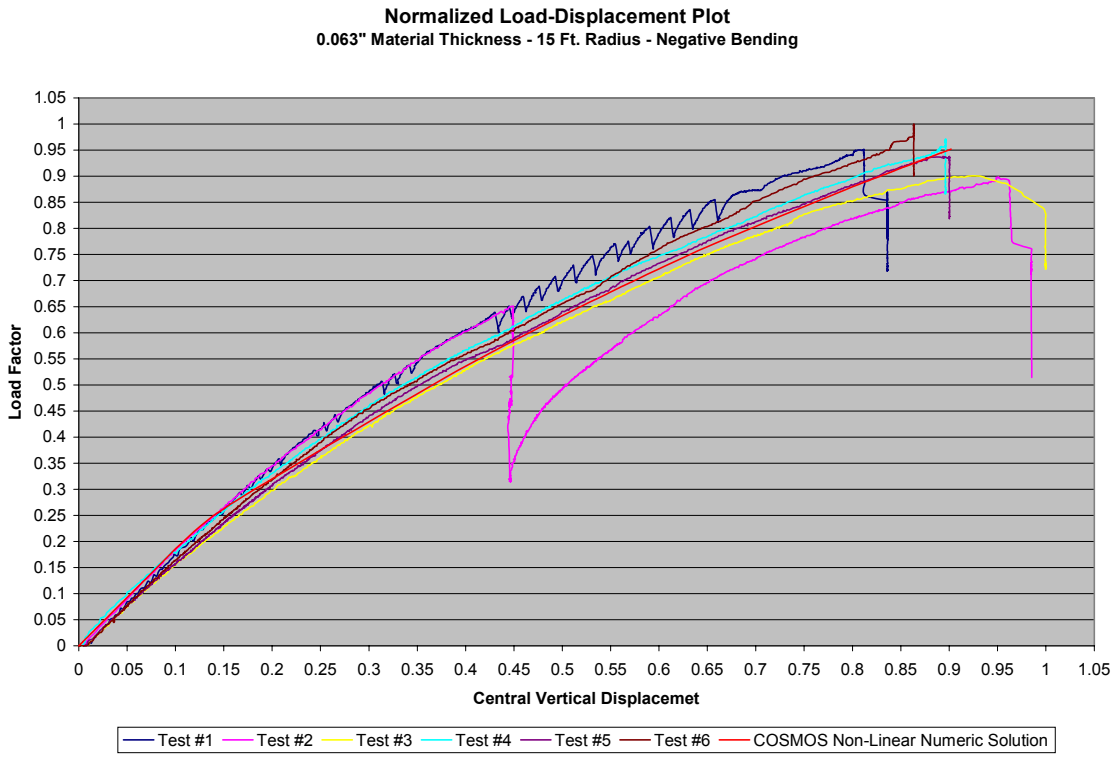

Figure 23 Load-Deflection Plot: 15-Foot Radius Panel with Numerical Prediction

Figure 23 is the last of the test series tested and modeled for this paper. The data is representative of a fifteen-foot radius panel. The test data showed very good agreement between each individual test, and the numerical solution was developed to adhere to the test data.

Due to the plots in this paper all being normalized for the individual test series being evaluated, it may be difficult to compare the relationship between the test series. To accomplish this, Figure 24 was developed which shows a normalized plot using the non-linear solutions from each of the five test series. Because the non-linear solution was established by developing a stiffness curve average of the each of the test series, the non-linear solutions are considered to be representative of an average of the test data.

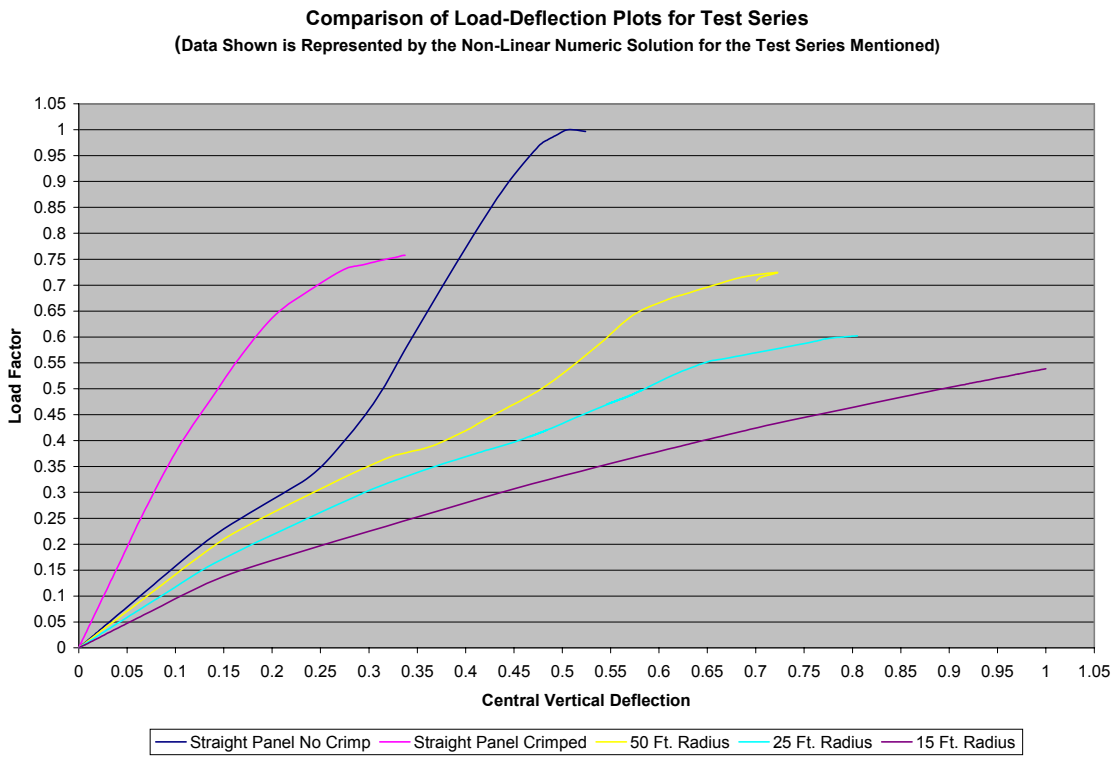

Figure 24 Comparison of Load-Deflection Curves for Entire Test Series

As shown in Figure 24, the curves all tend to follow a pattern as the radius of the panel changes. As expected, the loads become lower as the radius decreases. This is to be expected due to the crimp in the panel becoming deeper as the radius is decreased. The conclusion from this is that the crimp in the panel has a much larger affect than was once thought. An interesting note is that the straight, crimped panel, is shown to be somewhat stiffer than the rest of the panels. The corrugation is surmised to play a role in the apparent gain in stiffness. One will notice however, that as the crimps are deepened as evidenced by tighter radii, the slope drops back off to below the straight panel with no crimp.

As a separate check of the non-linear solution, Figure 25 shows a normalized plot of the derived stiffness curves used in the numerical analysis. From these derived curves, the effective modulus of elasticity for the panel can be calculated.

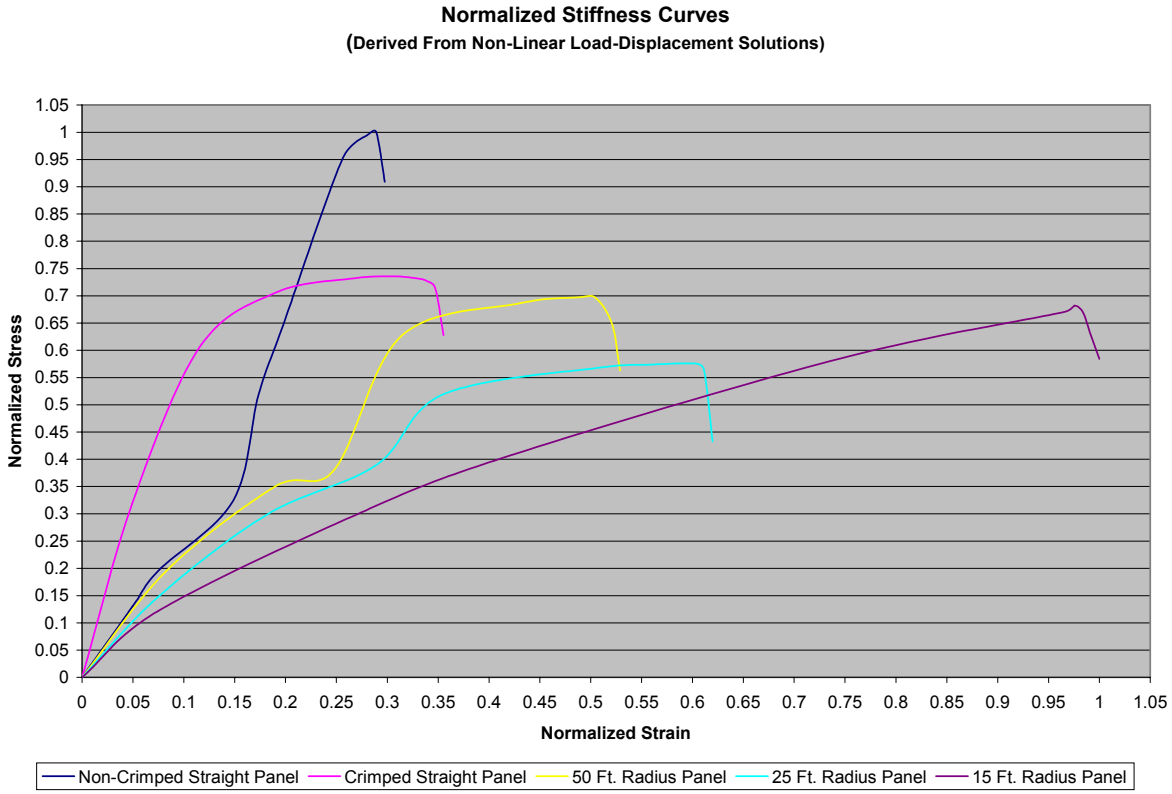

Figure 25 Derived Stiffness Curves (Normalized) Based on Actual Test Data

In conjunction with the curves from Figure 25, it is possible to check the analysis by using a well-known analytical linear solution for the linear portion of the curves. The check involves using Equation 1.

$$\Delta_{\max} = \frac{Pa}{24EI}\left(3L^2 - 4a^2\right) \qquad \textbf{Equation 1}$$

This equation solves the analytical linear equation that relates deflection, load, and modulus of elasticity. The parameters shown in Equation 1 are defined in Figure 26 [19].

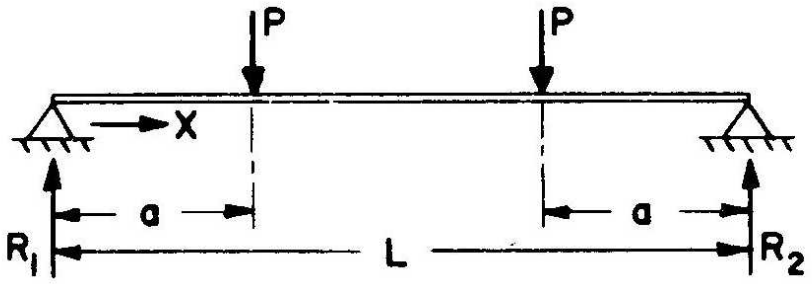

Figure 26 4 Point Bend Test Geometry Definitions

In addition to the geometric definitions found in Figure 26, the other parameters in Equation 1 are Δ_{max} for the maximum deflection, E representing the modulus of elasticity, and I representing the moment of inertia. By solving Equation 1 for E, and by substituting the actual values for all other parameters, the modulus of elasticity for the panel can be obtained. This check was performed using the actual values from the test data, and has shown that the analytical modulus of elasticity given by Equation 1, matches the modulus of elasticity as determined by the average of the derived stiffness curves to within 1%. This check serves as verification that the non-linear solution is correct.

4.0 OPTIMIZATION

During the optimization process, there are an infinite number of panel profiles one can test. The main goal of course, is to obtain a solution for a new panel profile that significantly increases the moment capacity of the panel currently in use while keeping the new profile simple enough for construction. In addition, although this paper dealt with negative bending tests, the optimization process will also use the eigenvalue solutions to attempt to achieve a balance for buckling loads between negative and positive bending. With this in mind, a modified profile of the current design was first chosen. The goal was to increase the local buckling factor of the panel. The profile chosen as a first initial run is shown in Figure 27.

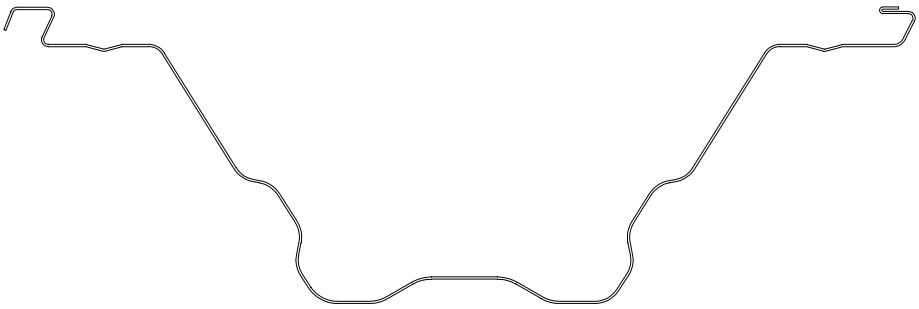

Figure 27 Optimized Structural Panel A

As shown in Figure 27, the panel has been modified by increasing the center stiffener in the middle belly of the panel, and also includes two deep side stiffeners. Because the 3-D beam element analyses were calibrated to actual test data, the optimization process cannot make use of this type of solution for a comparison study between potential new panel profiles. Rather, because of the good agreement seen by the explicit finite element model of the current panel, and

the use of an eigenvalue solution to extract a buckling load, this method will be utilized for the optimization process. All analyses were set up using the typical 4-point bend configuration, and the same boundary conditions from the original testing were used. A detailed model was developed for the optimized panel, herein called Panel A, and the results of the buckling mode are shown in Figure 28.

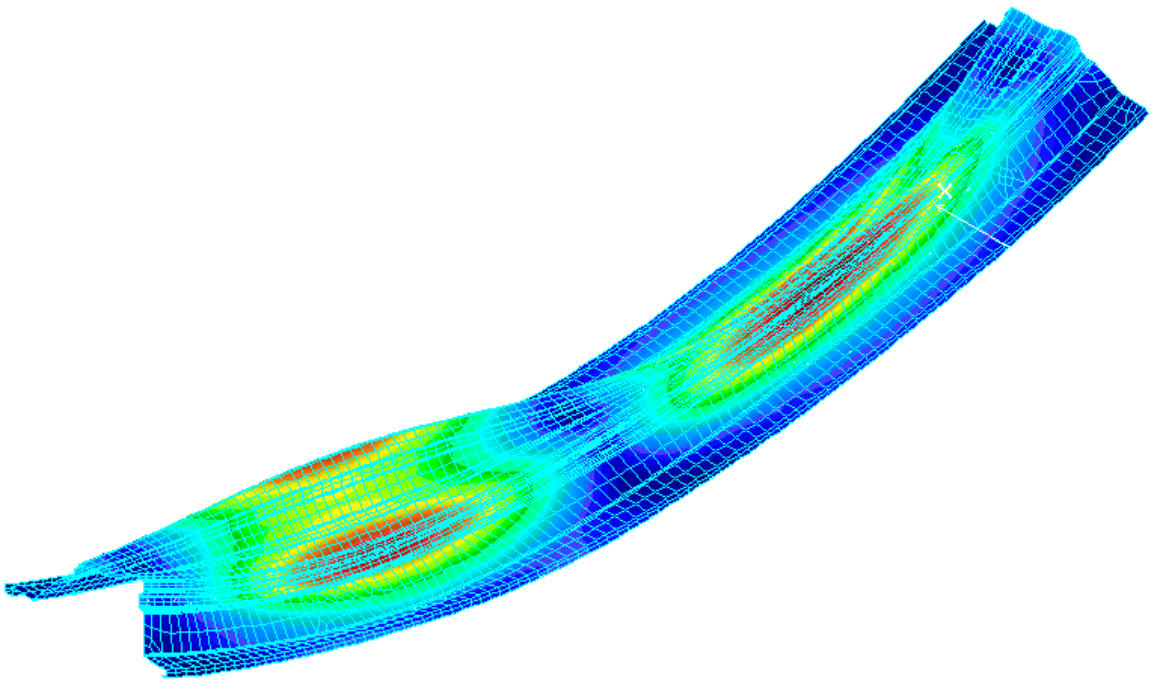

Figure 28 Eigenvalue Buckling Response for Panel A (Torsional)

As one can see, the response of the panel is not similar to the response of the current panel. Here, the first buckling mode, shown in Figure 28, predicts a torsional buckling failure, instead of the snap-thru type buckling failure. The model shown is for a fifty-foot radius panel. This radius was chosen for the optimization study due to this radius being an average between a straight panel and a tight radius panel. In comparison to the current panel at a fifty-foot radius, panel A exhibited an increase of 1.74 times over the current panel. The first instance for the

middle section to experience a buckling failure occurs during the third buckling mode. The load factor increase between the original panel, and the third mode buckling of panel A was 2.4. The buckling mode is shown in Figure 29.

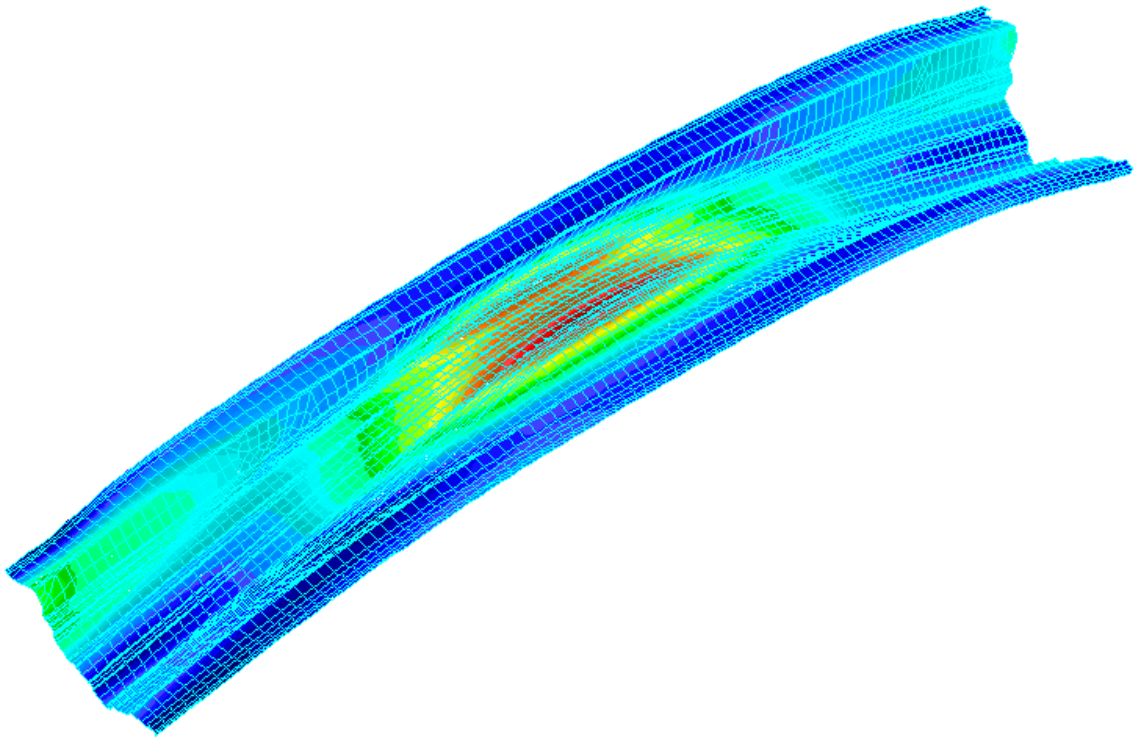

Figure 29 Eigenvalue Buckling Solution for Panel A (Middle Section Buckle)

The buckling mode shown in Figure 29 suggests that if the panel can be constrained from torsional buckling failure, and the buckling mode for a localized snap-thru type buckling is allowed to transpire, then a substantial load increase can be achieved. It can be shown in Figure 29, that the torsional component has disappeared from the panel, and that a more localized buckle occurs towards the center of the panel. As mentioned above, a balance between positive

and negative bending was also evaluated. The positive bending for Panel A is shown in Figure 30.

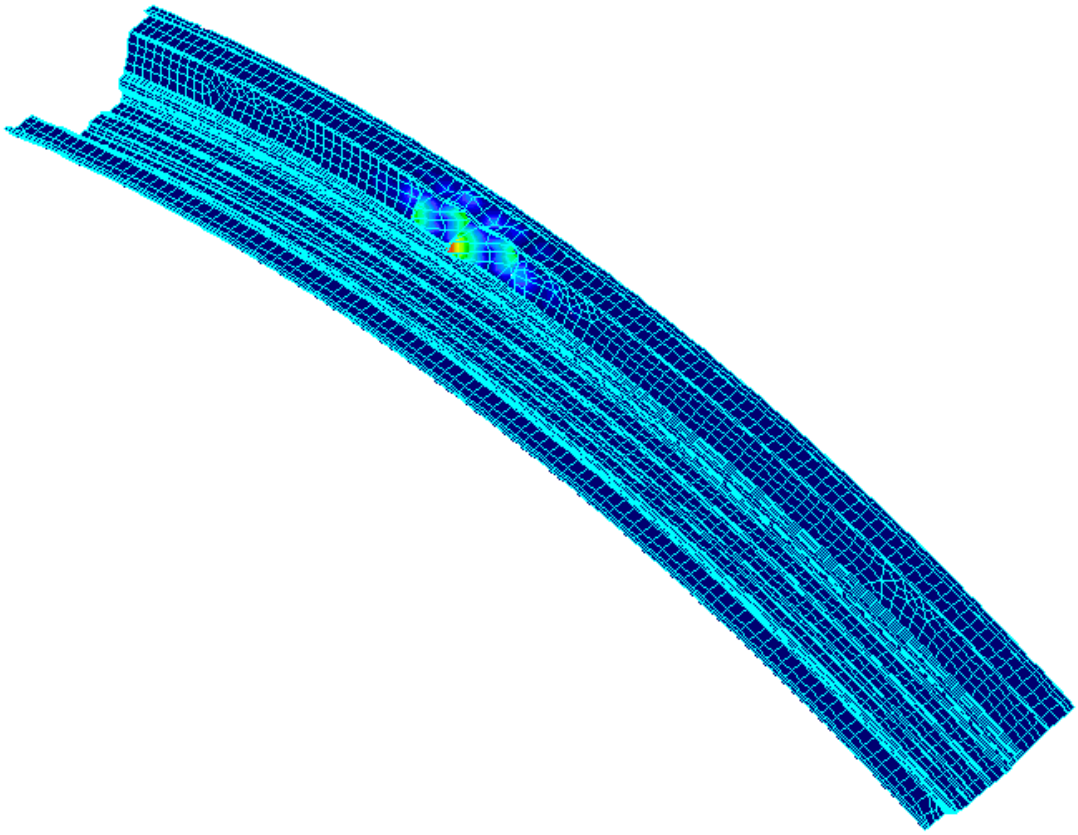

Figure 30 Positive Bending Failure Mode for Panel A

It is shown in Figure 30 that the buckling mode of failure appears in the upper flange of the panel. This failure is the expected method in which the panel will fail when introduced to positive bending. As a comparison to the current panel configuration, there is no substantial gain from the Panel A configuration and the current panel in positive bending. This finding alludes to the conclusion that this panel profile would not be a viable option for use as a replacement for the current panel configuration.

A second panel profile was tested, which was based on the current panel profile using a modified belly.

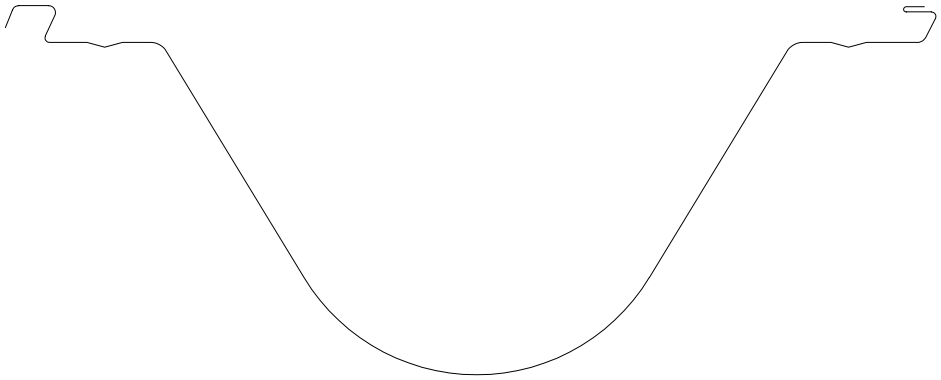

Figure 31 Optimized Structural Panel B

Figure 31 depicts the panel profile showing a modified belly in comparison to the current panel configuration. Upon initial test runs for this panel profile, it was quickly determined that the buckling load failure compared between negative and positive bending was again not in close agreement. Another problem with this type of profile is that if produced, difficulties in roll forming and corrugating the belly of the panel would be present. Because of these findings, this panel was also quickly abandoned as a possible replacement for the existing profile.

The last panel profile to be tested as a possible replacement is a radical change from the other panel profiles tested to this point. The profile consisted of securing the same hook and hem portions of the original panel, but instead of inclined web portions, the web was inclined to a completely vertical profile. In addition, the traditional belly of the panel was replaced with

multiple stiffeners that could be compared to thin deck plating. The profile for this design is shown in Figure 32.

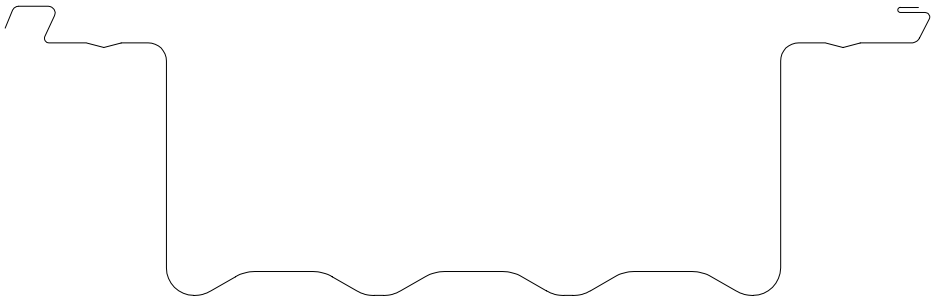

Figure 32 Optimized Structural Panel C

The panel was programmed into a finite element model in the same manner as the other profiles, along with the same boundary conditions and loading configuration. Upon evaluation using the eigensolver solution scheme, the predicted buckling load far exceeded expectations. In comparison to the present panel configuration, the negative bending increase was shown to be 4.95 times that of the current panel. In addition, the positive bending buckling load varied from the negative buckling load by only 4.5 percent. This indicates that the panel is well balanced between positive and negative bending. The predicted numerical solution for the negative bending case is shown in Figure 33. As one can see, the strength of the bottom belly portion of the panel becomes quite evident. The buckling mode in negative bending essentially causes the belly of the panel to heave as one unit, as opposed to the localized buckling of the current panel. The extra and deep stiffeners placed in the belly appear to have a large influence on how much capacity the panel can handle.

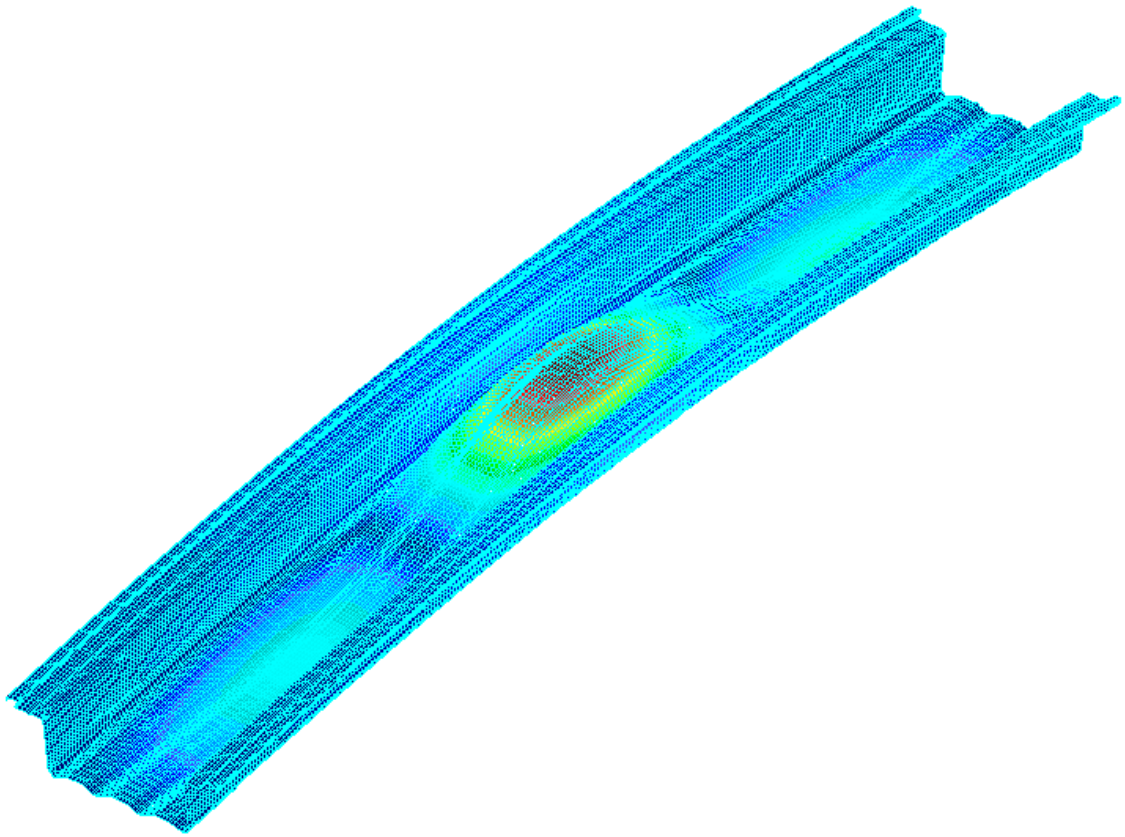

Figure 33 Eigenvalue Buckling Mode for Panel C (Negative Bending)

By contrast, the positive bending buckling mode is shown to be similar to the positive buckling mode seen for Panel A. The top flange buckles and failure occurs in the top portion of the web, along with failure in the hem portion of the panel. However, as mentioned earlier, the buckling loads for negative and positive bending are very similar for this panel configuration. Thus in theory, based on the eigenvalue solutions, the panel when in a service condition should be well balanced.

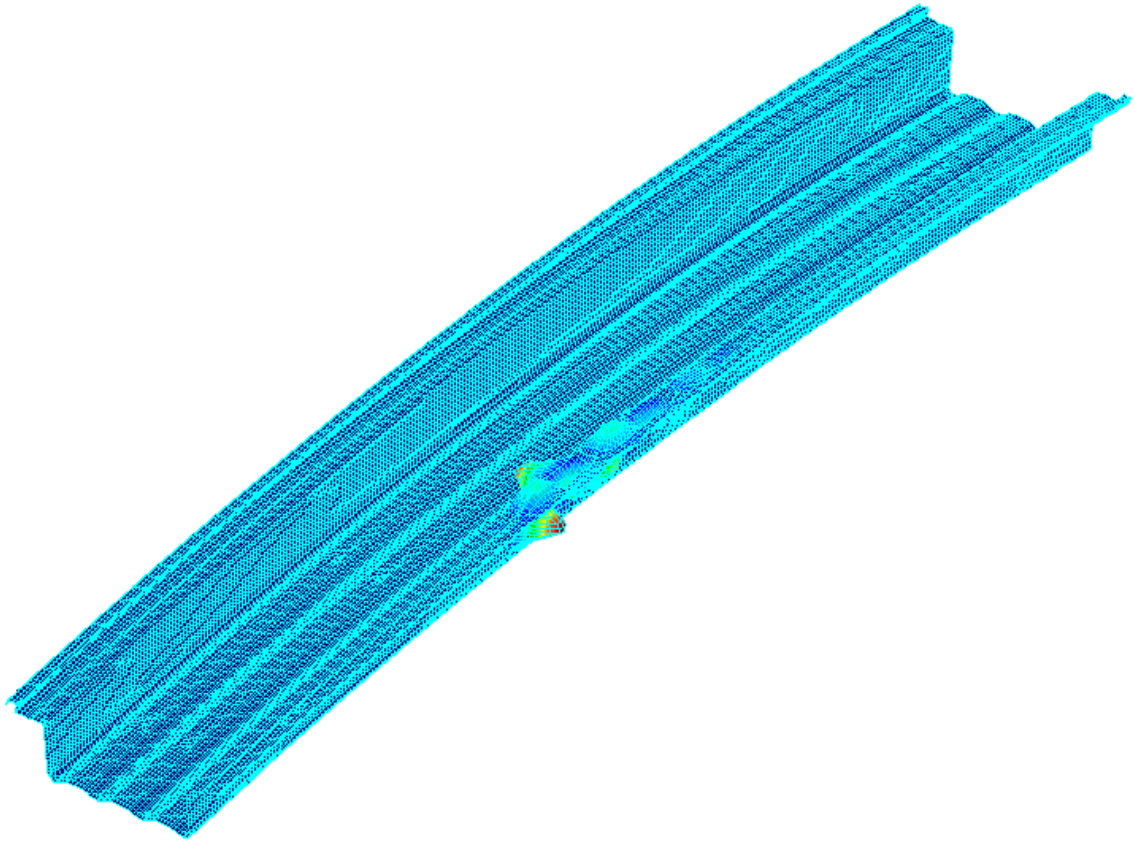

Figure 34 Eigenvalue Buckling Mode for Panel C (Positive Bending)

5.0 CONCLUSIONS

The conclusions based on this paper are as follows. It is possible to successfully model explicitly a panel profile that can be used for optimization studies for use as possible future test studies. It has also been shown, that if test data exists, a numerical solution can be very accurately modeled to match the test data by modifying the material properties of the model. This modification will take into account any stiffening effects, as well as the influence of geometric parameters that cannot be readily accounted for, such as panel corrugation. In addition, upon verification of a modified material stiffness curve which accurately matches recorded test data, the stiffness curves can be used to model full scale buildings by applying the characteristics of the stiffness curves to various portions of the full scale model. The claims made by other researchers stating that a linear elastic solution cannot be used to solve problems involving thin shell arch panels has been confirmed by the research in this paper. Rather, a non-linear solution is the most precise method for obtaining accurate solutions to the panel in question. For future tests, it is suggested to evaluate multiple material thickness panels to establish any existing relationship between material thickness and panel radius. It is surmised and theorized that the trend of ultimate failure load decreasing as radius is decreased will hold true for various material thickness. The theory stating that the loads will be lower if the material thickness is decreased, and the loads going higher if the material thickness is increased.

BIBLIOGRAPHY

1. George Abdel-Sayed, Frank Monasa, and Wayne Siddall. "Cold-Formed Steel Farm Structures Part II: Barrel Shells." *Journal of Structural Engineering* 111, no. 10 (Oct. 1985): 2090-2104.

2. Mohamed N. El-Atrouzy, and George Abdel-Sayed. "Prebuckling of Orthotropic Barrel-Shells." *Journal of the Structural Division* 104 (Nov. 1978): 1775-1786.

3. Ashutosh Bagchi, and V. Paramasivam. "Stability Analysis of Axisymmetric Thin Shells." *Journal of Engineering Mechanics* 122, no. 3 (March 1996): 278-281.

4. Yong-Lin Pi, and N.S. Trahair. "In-Plane Buckling and Design of Steel Arches." *Journal of Structural Engineering* 125, no. 11 (Nov. 1999): 1291-1298.

5. M.A. Bradford, B. Uy, and Y.-L. Pi. "In-Plane Stability of Arches under a Central Concentrated Load." *Journal of Engineering Mechanics* 128, no. 7 (July 2002): 710-719.

6. Steven Sweeney, Demetres Briassoulis, and Anthony Kao. "Evaluation of K-Span as a Rapidly Erectable Lightweight Mobilization Structure (RELMS)." US Army Corps of Engineers Construction Engineering Research Laboratory Technical Report M-91/06 (Jan. 1991)

7. Demetres Briassoulis, Anthony Kao, and Steven Sweeney. "Determination of the Ultimate Loads for Corrugated-Steel, Barrel-Type Shell Structures." US Army Corps of Engineers Construction Engineering Research Laboratory Technical Report M-88/01 (Oct. 1987)

8. MSC Software. "Case History: Equivalent Orthotropic Properties for Corrugated Sheets." 12 Sept. 2002 (http://www.mscsoftware.com.au/services/cases/macro/).

9. K.J.R. Rasmussen and G.J. Hancock. "Buckling analysis of thin-walled structures: numerical developments and applications." *Prog. Struct. Engng Mater* 2000, no. 2 (2000): 359-368.

10. S. Li, W. Hao, and W.K. Liu. "Numerical simulations of large deformation of thin shell structures using meshfree methods." *Computational Mechanics* 25 (2000): 102-116.

11. Mark Holst, J. Michael Rotter, and Chris R. Calladine. "Imperfections and buckling in cylindrical shells with consistent residual stresses." *Journal of Constructional Steel Research* 54 (2000): 265-282.

12. Michael Nemeth and James H. Starnes Jr. "The NASA Monographs on Shell Stability Design Recommendations." National Aeronautics and Space Administration Technical Report NASA/TP-1998-206290 (Jan. 1998)

13. Klaus-Jurgen Bathe, *Finite Element Procedures* (Upper Saddle River, New Jersey: Prentice-Hall, Inc., 1996).

14. Zhilun Xu, *Applied Elasticity* (New Delhi, India: Wiley Eastern Limited, 1992).

15. Alexander Blake, *Practical Stress Analysis in Engineering Design* (New York: Marcel Dekker, Inc., 1982).

16. Theodore V Galambos., ed. *Guide to Stability Design Criteria for Metal Structures Fifth Edition* (New York: John Wiley & Sons, Inc., 1998).

17. Wei-Wen Yu, *Cold-Formed Steel Design Second Edition* (New York: John Wiley & Sons, Inc., 1991).

18. "COSMOS/M 2.7 Non-Linear Structural Analysis" [electronic documentation manual] (Los Angeles, CA: Structural Research and Analysis Corporation, Dec. 2001)

19. The Aluminum Association, *Engineering data for aluminum structures Construction manual series Section 3 Fourth Edition* (Washington, D.C.: The Aluminum Association, Nov. 1981).